Janus Monolayers for Ultrafast and Directional Charge Transfer in Transition Metal Dichalcogenide Heterostructures

Ting Zheng,[†,‡] Yu-Chuan Lin,[*,¶,§] Neema Rafizadeh,[‡] David B. Geohegan,[¶] Zhenhua Ni,[*,†] Kai Xiao,[¶] and Hui Zhao[*,‡]

†*School of Physics and Key Laboratory of MEMS of the Ministry of Education, Southeast University, Nanjing 211189, China*

‡*Department of Physics and Astronomy, The University of Kansas, Lawrence, Kansas 66045, United States*

¶*Center for Nanophase Materials Sciences, Oak Ridge National Laboratory, Oak Ridge, Tennessee 37831, United States*

§*Department of Materials Science and Engineering, The Pennsylvania State University, University Park, Pennsylvania 16802, United States*

E-mail: yul194@psu.edu; zhni@seu.edu.cn; huizhao@ku.edu

Abstract

Charge transfer properties of van der Waals heterostructures formed by Janus and regular transition metal dichalcogenide monolayers are studied by time-resolved pump-probe measurements and photoluminescence spectroscopy. Measurements of electron and hole transfer in three heterostructures with atomic layer sequences of S-W-Se/S-W-S, Se-W-S/S-W-S, and S-W-Se/Se-W-Se reveal that charge transfer from regular to Janus monolayers is ultrafast regardless of the direction of the built-in electric field of

the Janus monolayer (Janus field). However, the charge transfer from Janus to regular layers is directional and controlled by the Janus field. When the current direction is along the field, the charge transfer is ultrafast and efficient, while the field blocks the charge transfer with an opposite charge current direction. The transferred carriers form interlayer excitons with extended lifetimes compared to the intralayer excitons. The demonstrated ultrafast and directional charge transfer between Janus and regular TMD layers introduces the Janus structures as an important building block for 2D heterostructures with efficient and directional charge transfer properties.

The recently developed van der Waals heterostructures[1–3] based on two-dimensional (2D) materials provide a new platform to understand, control, and utilize atomic-scale charge transfer phenomenon. Ultrafast charge transfer in various heterostructures has been observed[4,5] and was found to be insensitive to various parameters, such as the interlayer twist angle,[6–8] carrier kinetic energy,[9] lattice temperature,[10] and dielectric environments.[10] Such robust charge transfer is beneficial for harnessing emergent electronic and optical properties by integrating multiple 2D materials. However, effective control of this process is both fundamentally interesting and technologically relevant, as it represents the finest manipulation of charge motions at the nanoscale and enables various device designs, such as vertical tunneling transistors and photovoltaics.

Here we show that the built-in dipole electric field in Janus transition metal dichalcogenides (TMDs) can be utilized to control directional charge transfer in van der Waals heterostructures. A Janus TMD monolayer is composed of a TM atomic layer sandwiched by two different chalcogen atomic layers. Recently, Janus MoSSe and WSSe have been synthesized and characterized.[11–15] Due to its lattice asymmetry, a Janus TMD monolayer has a built-in electric field (which will be referred to as a Janus field hereafter) in the vertical direction. The Janus field can separate charge carriers to prolong their recombination lifetimes[16–18] and enhance the electron-phonon interaction.[19] By transient absorption measurements of charge transfer in three van der Waals heterostructures that combine Janus and

regular TMD monolayers, we find that charge transfer from Janus to regular TMD monolayers depends on the direction of the charge current relative to the Janus field direction. These results show that the Janus TMDs can be used as a building block to control the directional charge transfer properties in 2D heterostructures.

Results and Discussion

Janus-regular heterostructures and hypothesis on charge transfer

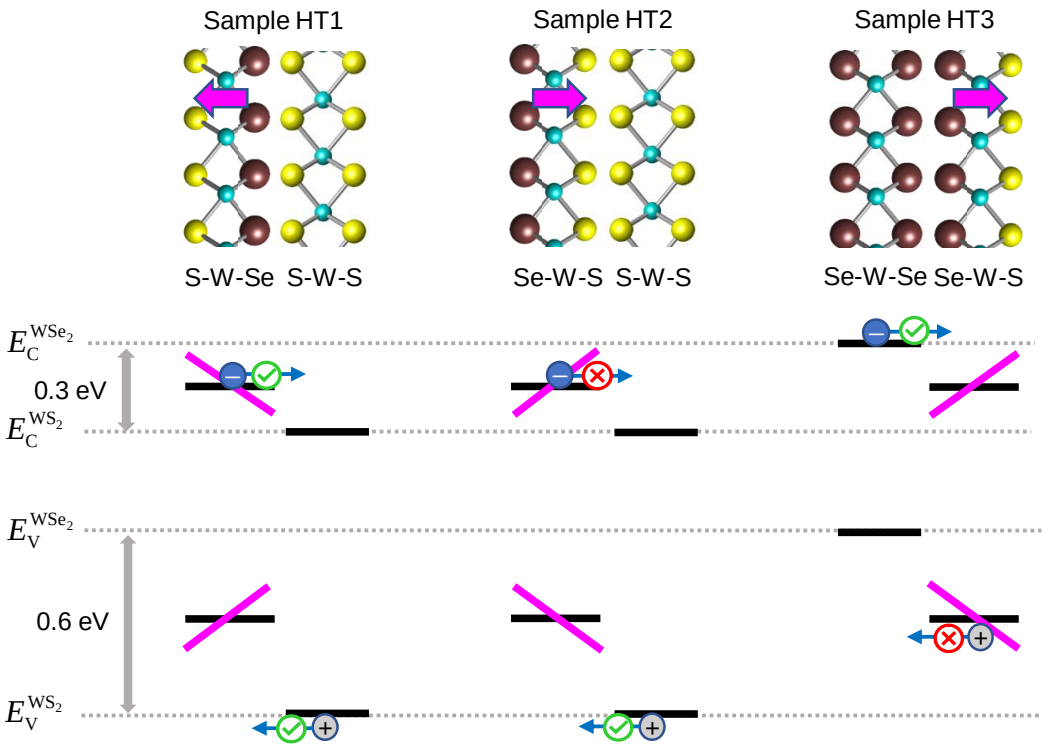

Figure 1: Top row: Crystal model of the three heterostructure samples studied. The magenta arrow indicates the built-in electric field in Janus WSSe. Bottom row: The band alignment of the three samples (solid black lines). The dotted lines represent the conduction band minima and valence band maxima of WS_2 and WSe_2, as labeled. The magenta lines illustrate change of the carrier potential energy across the Janus layer due to the Janus field.

Three Janus-regular TMD heterostructure samples are studied, as summarized in the top row of Figure 1. Sample HT1 has an atomic sequence of S-W-Se/S-W-S. The magenta arrow indicates the Janus field, which points from Se to S atomic layers. In the second

sample, HT2, with an atomic sequence of Se-W-S/S-W-S, the Janus field is reversed. The third sample (HT3, Se-W-Se/Se-W-S) differs from HT1 by changing the regular TMD from WS_2 to WSe_2. The bottom row of Figure 1 shows the expected band alignment of each sample. The dotted lines indicate (from top to bottom) the energies of the conduction band minima (CBMs) of WSe_2 ($E_C^{WSe_2}$) and WS_2 ($E_C^{WS_2}$), and the valence band maxima (VBMs) of them ($E_V^{WSe_2}$, $E_V^{WS_2}$), respectively. The offsets of the CB and VB are on the order of 0.3 and 0.6 eV, respectively, according to previous reports.[6,20] Since Janus WSSe has a band gap between that of WS_2 and WSe_2, we assume that its CBM and VBM are between those of WS_2 and WSe_2. As such, all three HTs are expected to form type-II band alignments, as indicated by the horizontal black lines in Figure 1.

Without the effect of the Janus field, the band alignment shown in Figure 1 is expected to drive electron (hole) transfer from left (right) to right (left) layers in all samples, as illustrated by the horizontal arrows. However, with a strong Janus field, the potential can change significantly across the Janus layer. Recent density functional theory studies have indicated that the Janus field can induce a potential drop of several hundred meV across a Janus TMD monolayer.[21–24] The magenta lines in the bottom row of Figure 1 illustrate schematically the potential energies of the electrons and holes in the Janus layers, or the band bending effect due to the Janus field. Along the field direction, the electric potential drops, and hence the potential energy of the holes (electrons) decreases (increases). We hypothesize that the Janus field is localized within the Janus layer and governs the flow of charge generated within the Janus layer, but is of insufficient strength to restrict interlayer charge injection. Specifically, for carrier transfer from Janus to regular TMDs, the Janus field allows (blocks) the transfer with the current direction along the same (opposite) direction of the field. Hence, the electron transfer from Janus to regular layers is allowed in HT1 but is blocked in HT2 by the energy barrier induced by the Janus field, while the hole transfer in HT3 is blocked by the Janus field. For carrier transfer from regular to Janus TMDs, Janus field allows charge transfer in both directions, which includes hole transfer in HT1 and HT2,

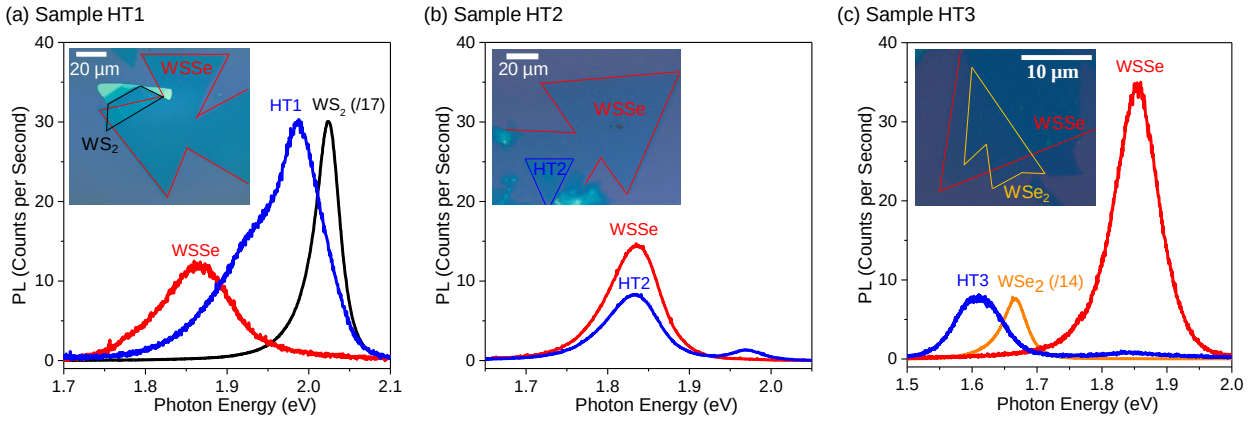

Figure 2: Photoluminescence (PL) spectra of the heterostructure sample HT1 (a), HT2 (b), and HT3 (c), all taken under the same excitation conditions of 3.06-eV continuous-wave laser with a power of 2.8 μW. The insets show the corresponding samples.

as well as electron transfer in HT3.

Samples and characterizations

To probe their interface quality and the charge transfer properties, Figure 2 shows the photoluminescence (PL) spectra of the heterostructure samples along with the corresponding monolayer regions, all measured under the continuous-wave laser excitation of 3.06-eV and 2.8 μW. The inset of Figure 2(a) is an optical microscope image of HT1, which is obtained by transferring a mechanically exfoliated monolayer WS_2 (the region enclosed by black lines) on top of a monolayer Janus WSSe flake (red lines). The spectra measured from different regions of the sample are shown in the main panel of Figure 2(a). The narrow PL peak of monolayer WS_2 at 2.02 eV (black, divided by 17) is consistent with previous reports.[25] The Janus WSSe region shows a broad PL peak at 1.87 eV (red).[18] The PL spectrum from HT1 (blue) has two components at 1.92 eV and 1.99 eV, respectively. They are assigned to the recombination of intralayer excitons in its WSSe and WS_2 layers, respectively. The large red (blue) shift of 30 (50) meV of the WS_2 (WSSe) peak could be attributed to the different dielectric environments and lattice strain compared to monolayer WS_2 (WSSe). The WS_2 peak is significantly quenched in HT1, while the 1.92-eV component shows a comparable

intensity as the 1.87-eV peak in WSSe monolayer. Figure 2(b) present the microscope image and the PL spectra of HT2, which is obtained by converting the topmost S layer of a bilayer WS_2 to Se. The WS_2 peak in HT2 is quenched by about 200 times compared to monolayer WS_2 [black curve in Figure 2(a)], while the WSSe peak is only moderately quenched. Finally, results from HT3, which is obtained by transferring an exfoliated WSe_2 monolayer onto a monolayer Janus WSSe flake, are shown in Figure 2(c). The PL of WSe_2 (orange) peaks at 1.67 eV, which is consistent with previously reported values.[26] The spectrum of Janus WSSe (orange) still shows a single peak at 1.86 eV. Two peaks are observed from the HT3 region (blue). The 1.84-eV peak is assigned to the intralayer excitons in WSSe, which is quenched by about 40 times. The 1.61-eV peak could be due to either the interlayer excitons or the shifted WSe_2 peak.

Charge transfer in HT1

The hypothesis on charge transfer is first tested by using sample HT1 with an atomic layer sequence of (from the substrate) S-W-Se/S-W-S. The type-II band alignment allows electron transfer from WSSe to WS_2. According to our hypothesis, such a transfer is allowed since its current direction is parallel to the Janus field, as shown in Figure 3(a). To study this process, a 1.86-eV and 0.31-ps pump pulse, which is tuned to the optical band gap of WSSe, selectively excites excitons in WSSe. The WS_2 layer is unexcited due to its larger optical band gap. The potential electron transfer to WS_2 is monitored by measuring differential reflectance (DR) of a 2.03-eV probe pulse (optical band gap of WS_2), which is defined as $\Delta R/R_0 = (R - R_0)/R_0$, where R and R_0 are the probe reflectance with and without the presence of the pump, respectively.

Before presenting the results from the HT1, we first discuss the control experiments performed on the individual WSSe and WS_2 monolayers, respectively. The black squares in Figure 3(b) and (c) show the signal from WSSe with a 54-μJ cm^{-2} pump pulse, which is attributed to the change of the reflectance of WSSe at the probe energy due to the excitons

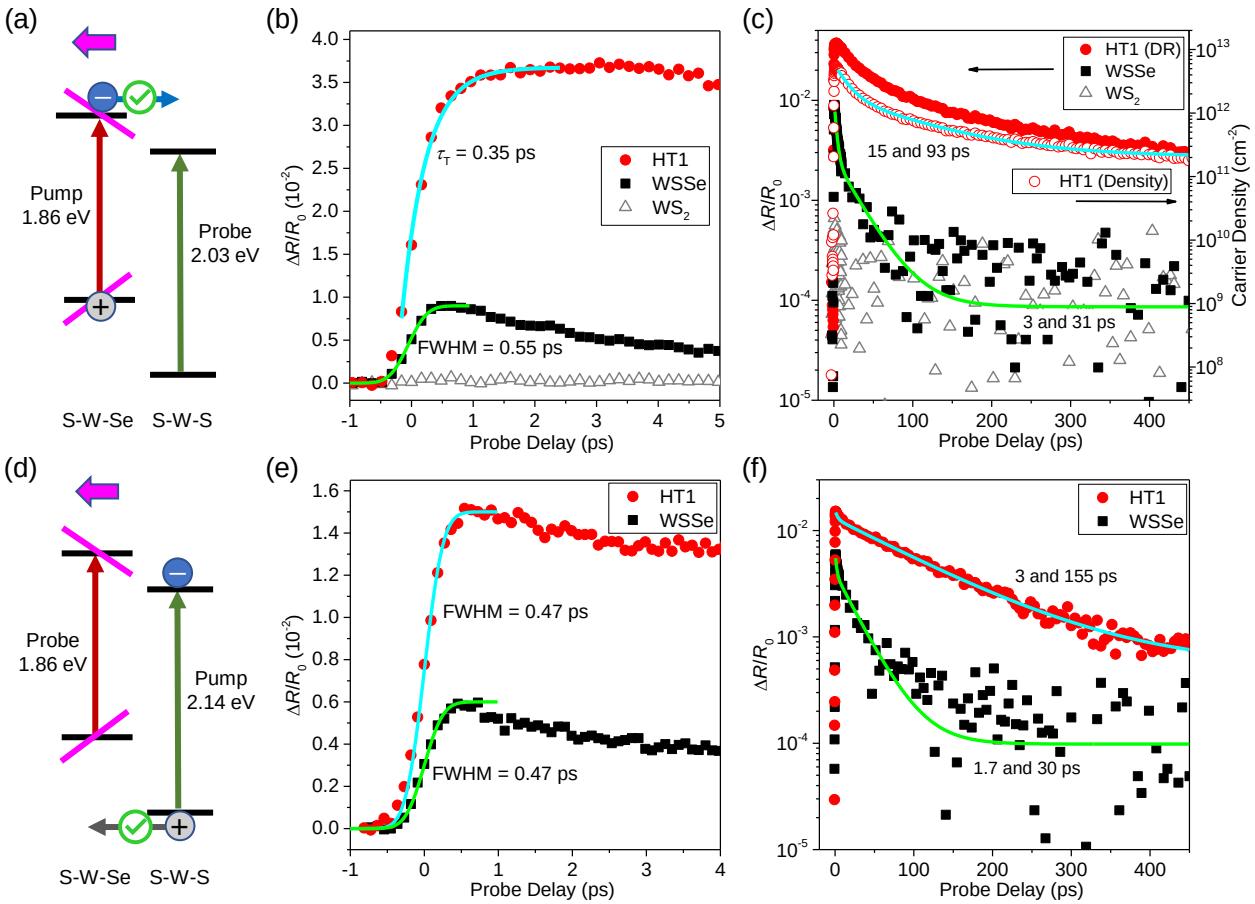

Figure 3: Directional charge transfer in S-W-Se/S-W-S heterostructure. (a) Band alignment of the heterostructure sample HT1. In the pump-probe experiments, a 1.86-eV pump pulse excites electrons in the WSSe layer. Their transfer to WS_2 is monitored by a 2.03-eV probe. The magenta lines illustrate change of the carrier potential energy due to the Janus field. (b) DR of the Janus WSSe monolayer (black), the WS_2 monolayer (gray), and the heterostructure (red). Curves are fits (see text). (c) Same as (b) but over a longer time range. The open red circles are the time-dependent carrier density in the WS_2 layer of the heterostructure (right axis). Curves are exponential fits (see text). (d) Configuration to study hole transfer from WS_2 to WSSe, with a 2.14-eV pump and a 1.86-eV probe. (e) DR of the Janus WSSe monolayer (black) and the HT1 (red), both with a pump fluence of 16 μJ cm^{-2}. Curves are fits (see text). (f) Same as (e) but over a longer time range. Curves are exponential fits (see text).

injected by the pump.[27] The signal rises to its peak rapidly, which can be fit by the integral of a Gaussian function with a full width at half maximum (FWHM) of 0.55 ps (the green curve). This time is slightly longer than the expected response time of the setup of about 0.45 ps, which reflects the thermalization of the resonantly injected excitons. When the same

measurement is performed on WS_2, no signal is detected, as indicated by the open triangles in Figure 3(b) and 3(c). The lack of signal confirms that the pump does not excite the WS_2 layer. The same measurement performed on HT1 produces a signal that is 4 times higher than that of WSSe, as shown by the red solid circles in Figure 3(b) and 3(c). This signal is mainly due to the electrons that are excited in WSSe and subsequentially transferred to WS_2, since without such transfer the signal from HT1 would have been similar to that of WSSe. The rise of the signal is noticeably slower than that of WSSe. A simple charge-transfer model, $N(t) = N_0[1 - \exp(-t/\tau_T)]$, can fit the rise well [cyan curve in Figure 3(b)]. Here, $N(t)$ represents the time-dependent electron density in WS_2, and N_0 is the maximal transferred density. The electron transfer time, τ_T, is found to be 0.35 ps from the fit.

In this measurement, the 54-μJ cm^{-2} pump pulse injects a peak carrier density of 5.4×10^{12} cm^{-2}, as estimated by using the absorbance of WSSe[18] of 0.013 at 1.86 eV. By repeating the measurement with various pump fluences, the transfer time is found to increase to 0.8 ps at low densities [see Figure S1(a)-S1(b)]. This result indicates that the carrier-carrier interaction could enhance interlayer charge transfer, which is consistent with results from regular TMD heterostructures.[28] By measuring the peak DR as a function of the injected density, we establish the relation between the signal and the carrier density as $\Delta R/R_0 = 0.065N/(N + N_s)$, where $N_s = (4.0 \pm 0.6) \times 10^{12}$ cm^{-2} [see Figure S1(c)]. This relation is used to convert the signal to the carrier density, as is shown by the open circles in Figure 3(c), and is fit by a biexponential function, $N(t) = N_0[A_1\exp(-t/\tau_1) + A_2\exp(-t/\tau_2) + B]$. Here, τ_1 and τ_2 describe the fast and slow components of the decay, with relative weights of A_1 and A_2, respectively. B is the weight of a time-independent component that could be due to lattice heating or carrier trapping effects. The fit (cyan curve) yields the two time constants (and their weights) of $\tau_1 = 15$ ps (63 %) and $\tau_2 = 93$ ps (33 %), along with $B = 4$ %. Furthermore, both time constants increase when lowering the injected carrier density [see Figure S1(f)]. τ_1 approaches 30 ps at low densities, and is assigned to the recombination of the intralayer excitons in WSSe. This component originates from regions of the sample with

accumulated interracial containment during annealing,[29,30] and thus low interface quality and inefficient electron transfer, where the sample behaves as two uncoupled monolayers.[5] τ_2 reaches about 200 ps at low densities and reflects the lifetime of the interlayer excitons formed by the transferred electrons in WS_2 and holes reside in WSSe. The decrease of these time constants at high densities is due to the contribution of exciton-exciton annihilation, which has been know to occur in TMD monolayers at such densities.[31–33] The results appear to suggest that the annihilation of interlayer excitons is similarly effective as the intralayer excitons. For comparison, the signal from WSSe is also fit by the same function, as shown by the green curve in Figure 3(c). The majority of the signal (71 %) decays with a constant of 3.0 ps, which can be attributed to the radiative recombination of the excitons that are injected in the light cone. Besides a small constant (1 %), the rest of the signal follows a 31-ps decay process, which is due to the nonradiative recombination of the excitons[18] and is consistent with the fast decay component of the signal from HT1. The charge transfer efficiency can be described by the percentage of the carriers that participate the transfer, which can is estimated by comparing the charge transfer time to the carrier lifetime. From the above results, we estimate that about 90 % of the excited electrons transfer. The efficiency could be further increased by exciting free carriers or excitons that are out of the light cone (and thus with longer effective lifetimes).

The band alignment of HT1 allows holes to transfer from WS_2 to WSSe. According to our hypothesis, such a regular-to-Janus transfer is not blocked by the Janus field. This process is studied by using the configuration illustrated in Figure 3(d). A 2.14-eV and 16-μJ cm^{-2} pump pulse injects excitons in both layers. With respective absorbances[18,34] of 0.009 and 0.006 for WSSe and WS_2 at 2.14 eV, respectively, the pump injects peak carrier densities of 9.6×10^{11} cm^{-2} and 6.4×10^{11} cm^{-2} in the WSSe and WS_2 layers, respectively. A 1.86-eV probe monitors the WSSe layer. We first discuss the control experiment performed on WSSe, as shown by the black squares in Figure 3(e) and 3(f). The rise of the signal follows the integral of a Gaussian function with a FWHM of 0.47 ps. The decay is biexponential

with two time constants, 1.7 ps (49 %) and 30 ps (50 %), and with a background of 1 %. The long time constant agrees well with that shown in Figure 3(c) and is attributed to the exciton lifetime in WSSe. The 1.7-ps process is attributed to exciton formation.[18] The red circles in Figure 3(e) and 3(f) show the signal of the same measurement of HT1. Compared to the electron transfer, this measurement is complicated since the pump also excites WSSe. Since the electrons excited in WSSe transfer to WS_2, without significant hole transfer to WSSe to compensate for the loss of electrons, the signal from the HT1 should be lower than that from WSSe. Hence, the enhanced signal observed in HT1 is strong evidence of hole transfer from WS_2 to WSSe. The rise of the signal can also be fit by the Gaussian integral of 0.47 ps. Since the signal near zero delay has contributions from the carrier injection in WSSe by the pump, the loss of electrons due to their transfer to WS_2, and the gain of holes that are transferred from WS_2, all of which occur on a time scale comparable to the pulse widths, the individual contributions are not separately resolvable. Rather, the hole transfer is manifested by the enhanced signal magnitude. The fast rise of the signal thus indicates an ultrafast hole transfer process from WS_2 to WSSe, as illustrated in Figure 3(d). By repeating these measurements with various pump fluences, we find that the peak DR from HT1 is proportional to the injected carrier density (See Figure S2). By biexponential fits to the decay curves, two time constants (and weights) of about 3 ps (70 %) and 155 ps (30 %) are deduced. The slow time constant is consistent with the results of the interlayer exciton lifetime shown in Figure 3(c) (by probing the electrons in WS_2).

Charge transfer in HT2

To further probe the influence of the Janus field on charge transfer, we now flip the Janus monolayer, and thus the field direction, in the second heterostructure sample (HT2) with a layer configuration of Se-W-S/S-W-S. With the same band alignment as HT1, the electron transfer from WSSe to WS_2 is still allowed by the band offset. However, according to our hypothesis, the Janus field prevents such transfer since its *current* direction is opposite to the

field, as illustrated in Figure 4(a). This heterostructure is studied with the same procedure as HT1 and under the same experimental conditions. The blue triangles in Figure 4(b) and 4(c) show the signal of the 2.03-eV probe with the 1.86-eV pump injecting excitons in WSSe. This signal is similar to that of monolayer WSSe (black symbols) but significantly different

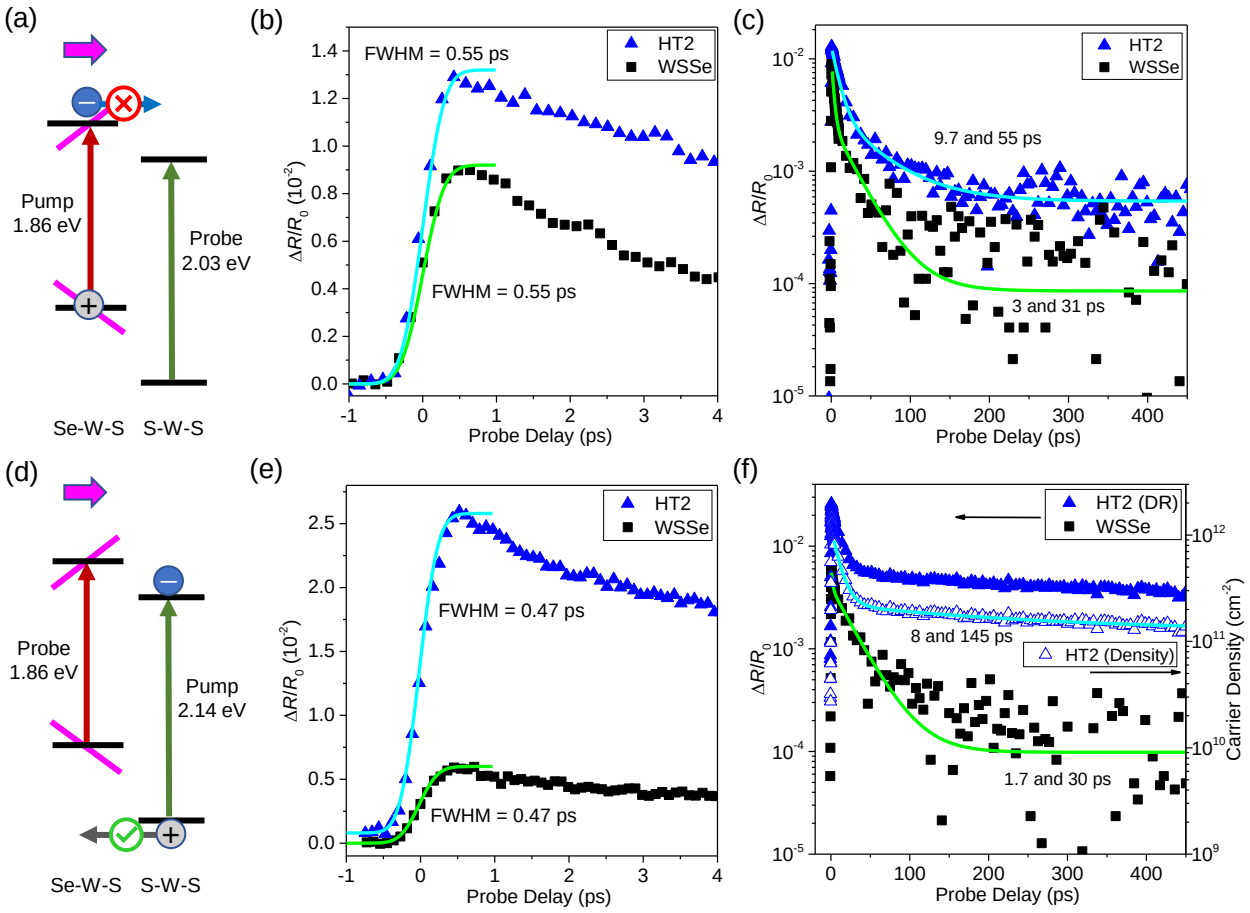

Figure 4: Directional charge transfer in Se-W-S/S-W-S heterostructure. (a) Band alignment of the heterostructure sample HT2. In the pump-probe experiments, a 1.86-eV pump pulse excites electrons in the WSSe layer. Their transfer to WS_2 is monitored by a 2.03-eV probe. The magenta lines illustrate change of the carrier potential energy due to the Janus field. (b) DR of the Janus WSSe monolayer (black) and the heterostructure (blue). Curves are fits (see text). (c) Same as (b) but over a longer time range. The open orange triangles are the time-dependent carrier density in the WSSe layer of the heterostructure (right axis). Curves are exponential fits (see text). (d) Configuration to study hole transfer from WS_2 to WSSe, with a 2.14-eV pump and a 1.86-eV probe. (e) DR of the Janus WSSe monolayer (black) and the HT2 (blue), both with a pump fluence of 16 μJ cm^{-2}. Curves are fits (see text). (f) Same as (e), but over a long time range. The open blue triangles are the time-dependent carrier density in the WSSe layer of the heterostructure (right axis). Curves are exponential fits (see text).

from that of HT1 [red symbols in Figure 3(b) and 3(c)], illustrating the pronounced effect of the Janus field direction. The rise of this signal is as fast as that of WSSe (0.55 ps, cyan and green curves), indicating that the signal is mainly due to the excitons directly injected in WSSe. The biexponential decay of this signal, with two time constants of 9.7 ps (71 %) and 55 ps (23 %) and with a background of 6 %, reflects the intralayer exciton dynamics in WSSe. All these features indicate that electrons excited in WSSe cannot transfer to WS_2 when the Janus field points towards the interface, as illustrated in Figure 4(a).

One key element of our hypothesis is that regular-to-Janus charge transfer is allowed, even if the current direction is opposite to the Janus field. This can be tested by studying the hole transfer from WS_2 to WSSe in HT2, as shown in Figure 4(d). To facilitate comparison, we used the same experimental conditions as HT1, where a 2.14-eV and 16 μJ cm^{-2} pump pulse excited both layers, while a 1.86-eV probe monitors the WSSe layer. The results are shown as the blue symbols in Figure 4(e) and 4(f), along with the previously discussed signal from WSSe (black squares, re-plotted from Figure 3). The signal from HT2 is about 4 times higher than that of WSSe, and with the same rise time. Its decay is much slower than that of WSSe, with a significant long-lived component. Since we have shown that the electron transfer from WSSe to WS_2 is insignificant in HT2, the signals from HT2 and WSSe should be similar if the holes excited in WS_2 could not transfer to WSSe. Hence, the enhanced signal in HT2 indicates efficient hole transfer from WS_2 to WSSe. Its resolution-limited rise time shows that the hole transfer is ultrafast. The peak signal (0.025) is higher than that of HT1 (0.015), which is consistent with the lack of electron transfer to WS_2 (and thus higher carrier density in the WSSe layer). Hence, the Janus field does not prevent hole transfer from WS_2 to WSSe even though its direction opposes the current direction. By repeating the measurement with various pump fluences, the relation between the signal and the carrier density is established [see Figure S3(b)], which is used to convert the signal to carrier density, as shown by the open triangles in Figure 4(f). The carrier density decays biexponentially (cyan curve) with two time constants of 8 ps (75 %) and 145 ps (11 %), which are attributed to the dynamics

of intralayer and interlayer excitons, respectively, along with a 14 % background.

It is worth noting that HT2 is fabricated by converting an AB-stacked bilayer WS_2, which is different from the dry transfer technique used for HT1. Therefore, the two layers in HT2 are expected to be well aligned, with strong interlayer coupling, while the twist angle of the two layers in HT1 (and HT3, to be discussed later) is random. However, previous studies have established that in TMD heterostructures, the ultrafast interlayer charge transfer is rather robust against the twist angles. For example, by studying a large number of MoS_2/WSe_2 heterostructure samples with various twist angles, it was found that the charge transfer time in all samples is shorter than 40 fs.[7] The PL quenching factor, which could be a good indicator of charge transfer time, was found to be rather consistent across more than 20 WS_2/WSe_2 samples with random twist angles.[6] The charge transfer time in 12 MoS_2/WS_2 samples (including CVD and transferred) with various twist angles was found to be all around 90 fs.[8] Hence, we do not expect the different twist angles in our samples to impact our study on their charge transfer properties.

Charge transfer in HT3

The hypothesis is further tested with a $WSSe/WSe_2$ heterostructure (HT3) that has a layer configuration of S-W-Se/Se-W-Se and a type-II type-II band alignment with the CBM and VBM in the WSSe and WSe_2 layers, respectively. Figure 5(a) illustrates the configuration to study electron transfer in HT3. Similar to the hole transfer studied in Figure 4(d), this is also a regular-to-Janus transfer with a current direction opposing the Janus field. In the experiment, electrons are excited in WSe_2 by a 1.66-eV pump pulse and their transfer to WSSe is monitored by a 1.82-eV probe pulse. The wine diamonds in Figure 5(b) and 5(c) show the results of the measurement performed on a WSe_2 monolayer. The 1.66-eV pump pulse with a peak fluence of 80 μJ cm^{-2} injects a peak carrier density of 2.1×10^{12} cm^{-2} in WSe_2, which has an absorbance of 0.03.[34] This signal originates from the induced reflectance change at 1.86 eV by the injected excitons. The rise of the signal follows the Gaussian integral

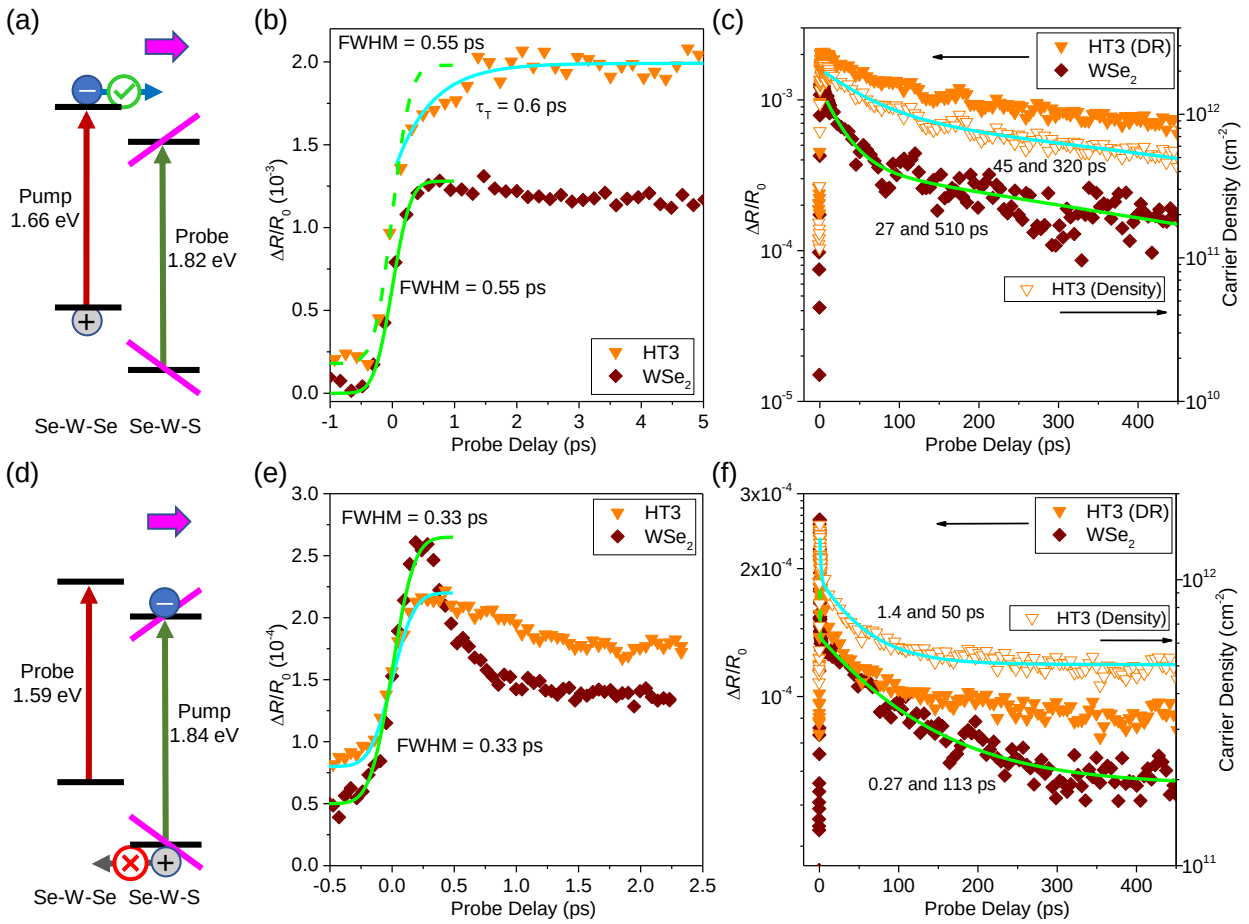

Figure 5: Directional charge transfer in Se-W-Se/Se-W-S heterostructure. (a) Band alignment of the heterostructure sample HT3. In the pump-probe experiments, a 1.66-eV pump pulse excites electrons in the WSe_2 layer. Their transfer to WSSe is monitored by a 1.82-eV probe. The magenta lines illustrate change of the carrier potential energy due to the Janus field. (b) DR of the WSe_2 monolayer (wine diamond) and the HT3 (orange triangles). Curves are fits (see text). (c) Same as (b) but over a 450-ps time range. The open triangles are the time-dependent carrier density in the WSSe layer of the heterostructure (right axis). Curves are exponential fits (see text). (d) Configuration to study hole transfer from WSSe to to WSe_2, with a 1.84-eV pump and a 1.59-eV probe. (e) DR of the WSe_2 monolayer (wine diamonds) and the HT3 (orange triangles), both with a pump fluence of 9.6 μJ cm^{-2}. Curves are fits (see text). (f) Same as (e) but over a long time range. The open triangles are the time-dependent carrier density in the WSe_2 layer of the heterostructure (right axis). Curves are exponential fits (see text).

with a width of 0.55 ps (green curve). The decay of the signal is biexponential [green curve in (c)], with two time constants of 27 ps (62 %) and 510 ps (38 %), and with a negligible background. The result from HT3 is shown by the orange triangles in Figure 5(b) and 5(c). Since the 1.66-eV pump does not excite WSSe, without electron transfer, the signal should be

similar to that from monolayer WSe_2. However, an enhanced signal with different temporal behaviors is observed. The signal enhancement is due to the transfer of electrons from WSe_2 to WSSe. The rise of the signal clearly shows two stages. The first part of the rise follows the 0.55-ps Gaussian integral well (dashed green curve) and represents the contribution from the excitons that are directly injected in WSe_2. The second stage can be described by the charge transfer model, as indicated by the cyan curve in Figure 5(b) with a charge transfer time of 0.6 ps. By varying the pump fluence, the charge transfer time is found to decrease with the injected carrier density [see Figure S4(b)]. This feature is similar to HT1. The signal is converted to the time-dependent carrier density (open symbols) by using the same procedure described above [Figure S4(c)], which decays biexponentially (cyan curve) with two time constants of 45 and 320 ps, respectively, due to recombination of the intralayer and interlayer excitons.

Finally, the hole transfer from WSSe to WSe_2 in HT3 is studied with the configuration shown in Figure 5(d). Such a transfer is band-offset-allowed but should be prevented by the Janus field, according to our hypothesis. A 1.84-eV and 9.6 μJ cm^{-2} pump pulse excites both layers, with peak carrier densities of 9.4×10^{11} and 5.7×10^{11} cm^{-2} in the WSSe and WSe_2 layers, respectively, which are estimated using their respective absorbances[18,34] of 0.013 and 0.008. A 1.59-eV probe monitors the carrier population in WSe_2. The wine diamonds in Figure 5(e) and 5(f) show the obtained signal when the measurement is performed on a WSe_2 monolayer. It rises to peak rapidly (green curve) and decays biexponentially (cyan curve) with two time constants of 0.27 ps (89 %) and 113 ps (9 %) and a background of 2 %. From HT3, a smaller signal is observed, as shown by the orange triangles. The signal reduction is consistent with the lack of hole transfer. For comparison, in HT1 and HT2 the hole transfer was found to be efficient enough to bring the signal above that of the corresponding monolayer. Through fluence-dependent measurements [Figure S5(b)], the signal is converted to the carrier density, which decays with two time constants of 1.4 ps (40 %) and 50 ps (30 %) and a long-lived background of 30 %. These features indicate the lack of hole transfer

from WSSe to WSe_2, further confirming our hypothesis.

Conclusion

In summary, we have studied charge transfer between Janus and regular TMD monolayers. We found by photoluminescence quenching and time-resolved pump-probe measurements that all three heterostructures studied have type-II band alignment in spite of the band bending effect in the Janus layer. We conclude that the Janus field is localized within the Janus layer and is of sufficient strength to govern the flow of charge generated within the Janus layer, but is of insufficient strength to restrict interlayer charge injection. The following features are consistently observed in all the heterostructures: First, the band-offset-allowed charge transfers from Janus to regular layers are directional: The Janus field allows the transfer with the charge current direction along the field while blocks that with opposite current direction. Second, the charge transfers from regular to Janus layers are unaffected by the Janus field and are similar to regular TMD heterostructures. Third, the transferred carriers form interlayer excitons with extended lifetimes compared to the intralayer excitons. Furthermore, the charge transfer speeds up with carrier density, suggesting robust charge transfer in high carrier injection levels. The ultrafast and directional charge transfer between Janus and regular TMD layers introduces the Janus structures as an important building block for 2D heterostructures with efficient and directional charge transfer properties. For example, the Janus field can enable charge transfer in type-I heterostructures by preventing transfer of one type of charge carriers, which is desirable for photovoltaic and photodetection applications. The additional control of charge transfer can also be utilized in vertical tunneling transistors.

Experimental Method

Fabrication of Janus WSSe monolayers WS_2 monolayers and bilayers grown by CVD on SiO_2/Si substrates are mounted on a 1-inch-diameter heater (Heat Wave Laboratories, Inc.) that is 10 cm away from the Se target in a cylindrical stainless-steel chamber (50 cm inner diameter, 36 cm tall). A 248-nm pulsed (25 ns) KrF laser with a repetition rate of 1-5 Hz is used to ablate a selenium pellet target (1-inch diameter, Plasmaterials, Inc., 99.99 % purity) in Ar gas, with a 1.25 mm $\times$ 4.5 mm rectangular spot. Typically, 57 mJ of energy is used to deliver a 1.0 J cm^{-2} pulse energy at the target surface. The heater temperature is PID controlled to $\pm$ 2°C with ramp-rates of about 30°C per minute. High-quality Janus WSSe is achieved with a pressure of 20 mTorr and a temperature of 300°C.

Fabrication of Janus-regular TMD heterostructures The heterostructure sample of HT1 is obtained by dry transferring an exfoliated WS_2 monolayer on top of a Janus WSSe monolayer, which is produced by the procedure described in the previous subsection. The monolayer of WS_2 is exfoliated from a bulk crystal (2D Semiconductors). After the transfer step, the sample is annealed at 200°C in Ar for 4 hours to obtain high interface quality,[35] which is confirmed by the significant photoluminescence (PL) quenching observed [Figure S1(c)]. The HT2 sample is fabricated by first growing a WS_2 bilayer flake by CVD, and then replacing its topmost S layer by low-energy Se-implantation described in the previous paragraph. The HT3 sample is fabricated by transferring an exfoliated monolayer from a bulk WSe_2 crystal (2D Semiconductors) onto a Janus WSSe monolayer, with the same procedure and annealing as HT1.

Micro-Photoluminescence spectroscopy Photoluminescence spectroscopy is performed with a homemade setup. A 405-nm continuous-wave diode laser (Thorlabs) is used for the excitation, which is focused on the sample surface with a spot size of about 1 μm by using an objective lens with a numerical aperture of 0.75. The PL is collected by the objective

lens and recorded by a spectrometer (Horiba iHR550) with a thermoelectrically cooled CCD camera (Synapse).

Differential reflection measurements Differential reflection measurements are performed with a homemade setup, which is based on a laser system including an 80 MHz and 100-fs Ti:sapphire oscillator, an optical parametric oscillator (OPO), a supercontinuum generator (SCG), and a second harmonic generator (SHG). For a certain measurement, two outputs of these devices are used as pump and probe pulses, which are combined by a beamsplitter and are co-focused on the sample to spot sizes of 1 - 2 μm by an objective lens. A mechanical chopper modulates the pump incident intensity at about 3 KHz. The reflected probe is collimated by the objective lens and measured by a silicon photodiode and a lock-in amplifier. With this setup, the DR of the probe is measured as a function of the time delay between the pump and probe pulses, $\Delta R/R_0 = (R - R_0)/R_0$, where R and R_0 are the reflectances of the sample with and without the presence of the pump beam, respectively.

Supporting Information Available

The Supporting Information is available free of charge at https://pubs.acs.org.

Additional power-dependent measurements on charge transfer in all heterostructure samples (PDF).

Acknowledgements

The ultrafast laser spectroscopy and PL measurements were supported by the U.S. Department of Energy, Office of Basic Energy Sciences, Division of Materials Sciences and Engineering under Award DE-SC0020995 and conducted at The University of Kansas. TZ and ZHN were supported by National Nature Science Foundation of China (61927808). The synthesis efforts and electron microscopy were supported by the U.S. Department of Energy,

Office of Basic Energy Sciences, Division of Materials Sciences and Engineering and conducted at the Center for Nanophase Materials Sciences, which is a DOE Office of Science User Facility.

References

1. Geim, A. K.; Grigorieva, I. V. Van der Waals Heterostructures. *Nature* **2013**, *499*, 419–425.

2. Liu, Y.; Weiss, N. O.; Duan, X.; Cheng, H.-C.; Huang, Y.; Duan, X. Van Der Waals Heterostructures and Devices. *Nat. Rev. Mater.* **2016**, *1*, 16042.

3. Mak, K. F.; Shan, J. Photonics and Optoelectronics of 2D Semiconductor Transition Metal Dichalcogenides. *Nat. Photonics* **2016**, *10*, 216–226.

4. Hong, X.; Kim, J.; Shi, S. F.; Zhang, Y.; Jin, C.; Sun, Y.; Tongay, S.; Wu, J.; Zhang, Y.; Wang, F. Ultrafast Charge Transfer in Atomically Thin MoS_2/WS_2 Heterostructures. *Nat. Nanotechnol.* **2014**, *9*, 682–686.

5. Ceballos, F.; Bellus, M. Z.; Chiu, H. Y.; Zhao, H. Ultrafast Charge Separation and Indirect Exciton Formation in a MoS_2-$MoSe_2$ van der Waals Heterostructure. *ACS Nano* **2014**, *8*, 12717–12724.

6. Wang, K.; Huang, B.; Tian, M.; Ceballos, F.; Lin, M.-W.; Mahjouri-Samani, M.; Boulesbaa, A.; Puretzky, A. A.; Rouleau, C. M.; Yoon, M.; Zhao, H.; Xiao, K.; Duscher, G.; Geohegan, D. B. Interlayer Coupling in Twisted WSe_2/WS_2 Bilayer Heterostructures Revealed by Optical Spectroscopy. *ACS Nano* **2016**, *10*, 6612–6622.

7. Zhu, H. M.; Wang, J.; Gong, Z. Z.; Kim, Y. D.; Hone, J.; Zhu, X. Y. Interfacial Charge Transfer Circumventing Momentum Mismatch at Two-Dimensional Van Der Waals Heterojunctions. *Nano Lett.* **2017**, *17*, 3591–3598.

8. Ji, Z. H.; Hong, H.; Zhang, J.; Zhang, Q.; Huang, W.; Cao, T.; Qiao, R. X.; Liu, C.; Liang, J.; Jin, C. H.; Jiao, L. Y.; Shi, K. B.; Meng, S.; Liu, K. H. Robust Stacking-Independent Ultrafast Charge Transfer in MoS_2/WS_2 Bilayers. *ACS Nano* **2017**, *11*, 12020–12026.

9. Ma, E. Y.; Guzelturk, B.; Li, G. Q.; Cao, L. Y.; Shen, Z. X.; Lindenberg, A. M.; Heinz, T. F. Recording Interfacial Currents on the Subnanometer Length and Femtosecond Time Scale by Terahertz Emission. *Sci. Adv.* **2019**, *5*, eaau0073.

10. Zhou, H. Z.; Zhao, Y. D.; Zhu, H. M. Dielectric Environment-Robust Ultrafast Charge Transfer between Two Atomic Layers. *J. Phys. Chem. Lett.* **2019**, *10*, 150–155.

11. Lu, A. Y.; Zhu, H. Y.; Xiao, J.; Chuu, C. P.; Han, Y. M.; Chiu, M. H.; Cheng, C. C.; Yang, C. W.; Wei, K. H.; Yang, Y. M.; Wang, Y.; Sokaras, D.; Nordlund, D.; Yang, P. D.; Muller, D. A.; Chou, M. Y.; Zhang, X.; Li, L. J. Janus Monolayers of Transition Metal Dichalcogenides. *Nat. Nanotechnol.* **2017**, *12*, 744–749.

12. Zhang, J.; Jia, S.; Kholmanov, I.; Dong, L.; Er, D. Q.; Chen, W. B.; Guo, H.; Jin, Z. H.; Shenoy, V. B.; Shi, L.; Lou, J. Janus Monolayer Transition-Metal Dichalcogenides. *ACS Nano* **2017**, *11*, 8192–8198.

13. Lin, Y.-C.; Liu, C.; Yu, Y.; Zarkadoula, E.; Yoon, M.; Puretzky, A. A.; Liang, L.; Kong, X.; Gu, Y.; Strasser, A.; Meyer, H. M.; Lorenz, M.; Chisholm, M. F.; Ivanov, I. N.; Rouleau, C. M.; Duscher, G.; Xiao, K.; Geohegan, D. B. Low Energy Implantation into Transition Metal Dichalcogenide Monolayers to Form Janus Structures. *ACS Nano* **2020**, *14*, 3896.

14. Petric, M. M.; Kremser, M.; Barbone, M.; Qin, Y.; Sayyad, Y.; Shen, Y. X.; Tongay, S.; Finley, J. J.; Botello-Mendez, A. R.; Muller, K. Raman Spectrum of Janus Transition Metal Dichalcogenide Monolayers WSSe and MoSSee. *Phys. Rev. B* **2021**, *103*, 035414.

15. Trivedi, D. B.; Turgut, G.; Qin, Y.; Sayyad, M. Y.; Hajra, D.; Howell, M.; Liu, L.; Yang, S. J.; Patoary, N. H.; Li, H.; Petric, M. M.; Meyer, M.; Kremser, M.; Barbone, M.; Soavi, G.; Stier, A. V.; Muller, K.; Yang, S. Z.; Esqueda, I. S.; Zhuang, H. L. *et al.* Room-Temperature Synthesis of 2D Janus Crystals and Their Heterostructures. *Adv. Mater.* *32*, 2006320.

16. Li, F. P.; Wei, W.; Wang, H.; Huang, B. B.; Dai, Y.; Jacob, T. Intrinsic Electric Field-Induced Properties in Janus MoSSe Van Der Waals Structures. *J. Phys. Chem. Lett.* **2019**, *10*, 559–565.

17. Ma, X. C.; Wu, X.; Wang, H. D.; Wang, Y. C. A Janus Mosse Monolayer: A Potential Wide Solar-Spectrum Water-Splitting Photocatalyst with a Low Carrier Recombination Rate. *J. Mater. Chem. A* **2018**, *6*, 2295–2301.

18. Zheng, T.; Lin, Y.-C.; Yu, Y. L.; Valencia-Acuna, P.; Puretzky, A. A.; Torsi, R.; Liu, C. Z.; Ivanov, I. N.; Duscher, G.; Geohegan, D. B.; Ni, Z. H.; Xiao, K.; Zhao, H. Excitonic Dynamics in Janus MoSSe and WSSe Monolayers. *Nano Lett.* **2021**, *21*, 931–937.

19. Guo, R.; Bu, X.; Wang, S.; Zhao, G. Enhanced Electron–Phonon Scattering in Janus MoSSe. *New J. Phys.* **2019**, *21*, 113040.

20. Kang, J.; Tongay, S.; Zhou, J.; Li, J. B.; Wu, J. Q. Band Offsets and Heterostructures of Two-Dimensional Semiconductors. *Appl. Phys. Lett.* **2013**, *102*, 012111.

21. Xia, C.; Xiong, W.; Du, J.; Wang, T.; Peng, Y.; Li, J. Universality of Electronic Characteristics and Photocatalyst Applications in the Two-Dimensional Janus Transition Metal Dichalcogenides. *Phys. Rev. B* **2018**, *98*, 165424.

22. Riis-Jensen, A. C.; Pandey, M.; Thygesen, K. S. Efficient Charge Separation in 2D Janus van Der Waals Structures with Built-in Electric Fields and Intrinsic P-N Doping. *J. Phy. Chem. C* **2018**, *122*, 24520–24526.

23. Riis-Jensen, A. C.; Manti, S.; Thygesen, K. S. Engineering Atomically Sharp Potential Steps and Band Alignment at Solid Interfaces Using 2D Janus Layers. *J. Phys. Chem. C* **2020**, *124*, 9572–9580.

24. Zhang, K.; Guo, Y.; Larson, D. T.; Zhu, Z.; Fang, S.; Kaxiras, E.; Kong, J.; Huang, S. Spectroscopic Signatures of Interlayer Coupling in Janus MoSSe/MoS_2 Heterostructures. *ACS Nano* **2021**, *15*, 14394–14403.

25. Ceballos, F.; Zereshki, P.; Zhao, H. Separating Electrons and Holes by Monolayer Increments in van der Waals Heterostructures. *Phys. Rev. Mater.* **2017**, *1*, 044001.

26. Cui, Q.; Ceballos, F.; Kumar, N.; Zhao, H. Transient absorption microscopy of monolayer and bulk WSe_2. *ACS Nano* **2014**, *8*, 2970–2976.

27. Ceballos, F.; Zhao, H. Ultrafast Laser Spectroscopy of Two-Dimensional Materials beyond Graphene. *Adv. Funct. Mater.* **2017**, *27*, 1604509.

28. Zereshki, P.; Valencia-Acuna, P.; Zhao, H. All-optical control of charge transfer and interlayer excitons in transition metal dichalcogenide heterostructures. *Phys. Rev. B* **2021**, *103*, 165416.

29. Haigh, S. J.; Gholinia, A.; Jalil, R.; Romani, S.; Britnell, L.; Elias, D. C.; Novoselov, K. S.; Ponomarenko, L. A.; Geim, A. K.; Gorbachev, R. Cross-Sectional Imaging of Individual Layers and Buried Interfaces of Graphene-Based Heterostructures and Superlattices. *Nat. Mater.* **2012**, *11*, 764–767.

30. Kim, Y.; Herlinger, P.; Taniguchi, T.; Watanabe, K.; Smet, J. H. Reliable Postprocessing Improvement of van der Waals Heterostructures. *ACS Nano* **2019**, *13*, 14182–14190.

31. Kumar, N.; Cui, Q.; Ceballos, F.; He, D.; Wang, Y.; Zhao, H. Exciton-Exciton Annihilation in $MoSe_2$ Monolayers. *Phys. Rev. B* **2014**, *89*, 125427.

32. Sun, D.; Rao, Y.; Reider, G. A.; Chen, G.; You, Y.; Brezin, L.; Harutyunyan, A. R.; Heinz, T. F. Observation of Rapid Exciton-Exciton Annihilation in Monolayer Molybdenum Disulfide. *Nano Lett.* **2014**, *14*, 5625–5629.

33. Yu, Y. L.; Yu, Y. F.; Xu, C.; Barrette, A.; Gundogdu, K.; Cao, L. Y. Fundamental Limits of Exciton-Exciton Annihilation for Light Emission in Transition Metal Dichalcogenide Monolayers. *Phys. Rev. B* **2016**, *93*, 201111.

34. Li, Y.; Chernikov, A.; Zhang, X.; Rigosi, A.; Hill, H. M.; van der Zande, A. M.; Chenet, D. A.; Shih, E.-M.; Hone, J.; Heinz, T. F. Measurement of the Optical Dielectric Function of Monolayer Transition-Metal Dichalcogenides: MoS_2, $MoSe_2$, WS_2, and WSe_2. *Phys. Rev. B* **2014**, *90*, 205422.

35. Purdie, D. G.; Pugno, N. M.; Taniguchi, T.; Watanabe, K.; Ferrari, A. C.; Lombardo, A. Cleaning Interfaces in Layered Materials Heterostructures. *Nat. Commun.* **2018**, *9*, 5387.

TOC Graphic

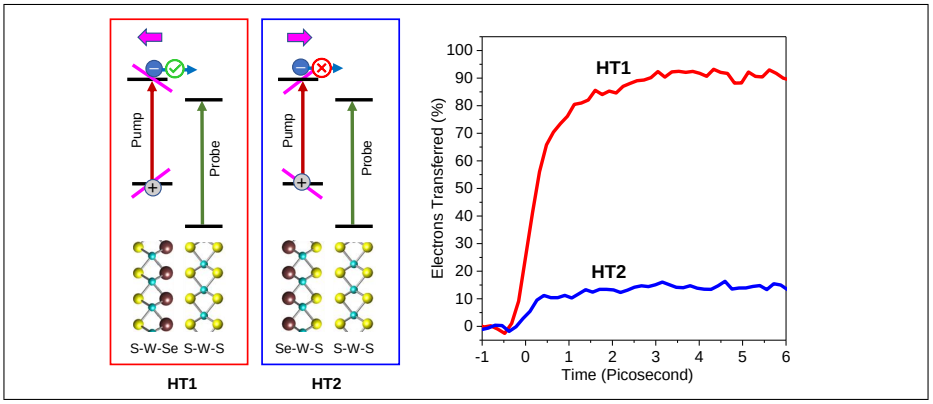
Pump
Probe
S-W-Se S-W-S
HT1
Pump
Probe
Se-W-S S-W-S
HT2
HT1
HT2
Electrons Transferred (%)
Time (Picosecond)
100
90
80
70
60
50
40
30
20
10
0
-1
0
1
2
3
4
5
6